Title

Blocking mitochondrial Zn2+ accumulation after ischemia reduces mitochondrial dysfunction and neuronal injury.

Journal

Journal of Neuroscience, 42(26)

ISSN

0270-6474

Authors

Medvedeva, Yuliya V
Yin, Hong Z
Bazrafkan, Afsheen
et al.

Publication Date

2022-06-29

DOI

10.1523/jneurosci.0874-21.2022

Peer reviewed

Neurobiology of Disease

Blocking Mitochondrial Zn^{2+} Accumulation after Ischemia Reduces Mitochondrial Dysfunction and Neuronal Injury

Yuliya V. Medvedeva,[1] Hong Z. Yin,[1] Afsheen Bazrafkan,[1] Andriy Yeromin,[2] Sung G. Ji,[3] Eli J. Weiss-Hung,[1] Edward Sharman,[1] Alyssa P. Avilez,[1] Niki Maki,[1] Masih A. Rafi,[1] Guilian Tian,[1] Yama Akbari,[1,3,4,5] and John H. Weiss[1,3]

[1]Departments of Neurology, [2]Physiology and Biophysics, [3]Anatomy & Neurobiology, [4]Neurological surgery, and [5]Beckman Laser Institute & Medical Clinic, University of California Irvine, Irvine, California 92697

Zn^{2+} is an important contributor to ischemic brain injury, and recent studies support the hypothesis that mitochondria are key sites of its injurious effects. In murine hippocampal slices (both sexes) subjected to oxygen glucose deprivation (OGD), we found that Zn^{2+} accumulation and its entry into mitochondria precedes and contributes to the induction of acute neuronal death. In addition, if the ischemic episode is short (and sublethal), there is ongoing Zn^{2+} accumulation in CA1 mitochondria after OGD that may contribute to their delayed dysfunction. Using this slice model of sublethal OGD, we have examined Zn^{2+} contributions to the progression of changes evoked by OGD and occurring over 4-5 h. We detected progressive mitochondrial depolarization occurring from ~2 h after ischemia, a large increase in spontaneous synaptic activity between 2 and 3 h, and mitochondrial swelling and fragmentation at 4 h. Blockade of the primary route for Zn^{2+} entry, the mitochondrial Ca^{2+} uniporter (with ruthenium red [RR]) or Zn^{2+} chelation shortly after OGD withdrawal substantially attenuated the mitochondrial depolarization and the changes in synaptic activity. RR also largely reversed the mitochondrial swelling. Finally, using an *in vivo* rat (male) asphyxial cardiac arrest model of transient global ischemia, we found that ~8 min asphyxia induces considerable injury of CA1 neurons 4 h later that is associated with strong Zn^{2+} accumulation within many damaged mitochondria. These effects were substantially attenuated by infusion of RR on reperfusion. Our findings highlight mitochondrial Zn^{2+} accumulation after ischemia as a possible target for neuroprotective therapy.

Key words: **hippocampal slice; ischemia; mitochondria; mitochondrial Ca^{2+} uniporter; oxygen glucose deprivation; zinc**

Significance Statement

Brain ischemia is a leading cause of mortality and long-term disability that still lacks effective treatment. After transient ischemia, delayed death of neurons occurs in vulnerable brain regions. There is a critical need to understand mechanisms of this delayed neurodegeneration which can be targeted for neuroprotection. We found progressive and long-lasting mitochondrial Zn^{2+} accumulation to occur in highly vulnerable CA1 neurons after ischemia. Here we demonstrate that this Zn^{2+} accumulation contributes strongly to deleterious events occurring after ischemia, including mitochondrial dysfunction, swelling, and structural changes. We suggest that this mitochondrial Zn^{2+} entry may constitute a promising target for development of therapeutic interventions to be delivered after termination of an episode of transient global ischemia.

Introduction

Brain ischemia is a leading cause of morbidity and mortality of the aging population for which there are no effective neuroprotective interventions (Hosseini et al., 2020). Hippocampal pyramidal neurons are highly vulnerable to injury. CA3 neurons selectively degenerate after limbic seizures (Ben-Ari et al., 1980a, b; Tanaka et al., 1988). In contrast, CA1 neurons were found to undergo distinctive delayed degeneration days after transient episodes of ischemia in both humans (Zola-Morgan et al., 1986; Petito et al., 1987) and rodents (Kirino, 1982; Ordy et al., 1993; Sugawara et al., 1999). Considerable evidence has accumulated supporting critical contributions of Zn^{2+} in this injury. While there are large amounts of Zn^{2+} in the brain (>100 μM), the vast

Received Apr. 22, 2021; revised Apr. 22, 2022; accepted May 18, 2022.

Author contributions: Y.V.M., H.Z.Y., Y.A., and J.H.W. designed research; Y.V.M., H.Z.Y., A.B., A.P.A., N.M., M.A.R., and G.T. performed research; Y.V.M., H.Z.Y., A.Y., S.G.J., E.J.W.-H., and E.S. analyzed data; Y.V.M., A.B., and J.H.W. edited the paper; Y.V.M. and J.H.W. wrote the paper.

This work was supported by National Institutes of Health Grants NS096987, NS100494, and NS121227 to J.H.W.; and American Heart Association Grant 17GRNT33410181 to J.H.W. We thank the University of California Irvine Center for Statistical Consulting; and Prof. Bruckner at University of California Irvine Public Health for valuable consultation and suggestions for statistical analysis.

The authors declare no competing financial interests.

Correspondence should be addressed to John H. Weiss at jweiss@uci.edu.

https://doi.org/10.1523/JNEUROSCI.0874-21.2022

majority of it is normally bound or sequestered such that free reactive Zn^{2+} is very low (subnanomolar). However, after ischemia considerable free Zn^{2+} was found to accumulate in vulnerable neuronal populations *in vivo* (Tonder et al., 1990). Further studies established that Zn^{2+} chelation is protective, implicating a Zn^{2+} contribution to the ischemic neurodegeneration (Koh et al., 1996; Calderone et al., 2004). Considerable evidence supports mitochondria as critical targets for the injury-promoting effects of Zn^{2+} (Shuttleworth and Weiss, 2011; Ji et al., 2019). Zn^{2+} can quickly enter the mitochondria via the mitochondrial Ca^{2+} uniporter (MCU) where it was shown to trigger multiple deleterious effects including mitochondrial depolarization, swelling, ROS generation, and irreversible inhibition of major mitochondrial enzymes (Saris and Niva, 1994; Sensi et al., 1999; D. Jiang et al., 2001; Sensi et al., 2003; Gazaryan et al., 2007; Ji and Weiss, 2018; Ji et al., 2020). Indeed, *in vivo* studies found considerable Zn^{2+} accumulation in hippocampal neuronal mitochondria after global brain ischemia which correlates with mitochondrial structural damage (including swelling), activation of large multiconductance channels, and release of proapoptotic peptides (Calderone et al., 2004; Bonanni et al., 2006; Yin et al., 2019).

To find effective treatments that can prevent delayed neuronal injury after ischemia, it is crucial to understand the sequence of events leading to irreversible changes. Acute hippocampal slices subjected to oxygen glucose deprivation (OGD) provide a valuable model to study such events: they have preserved neuronal networks and Zn^{2+} stores and thereby reproduce some critical aspects of *in vivo* ischemia while allowing continuous monitoring from single neurons. Our recent studies found that short episodes of OGD (~7-9 min, a few minutes shorter than needed to evoke acute cell death) trigger delayed and long-lasting (at least 1 h) Zn^{2+} accumulation in mitochondria of CA1, but not in CA3 neurons (Medvedeva et al., 2017). We considered whether this Zn^{2+} accumulation might be responsible for the high susceptibility of CA1 neurons to delayed ischemic degeneration. We further found that the Zn^{2+} accumulates through the MCU (Medvedeva et al., 2017), leading to the hypothesis that the MCU constitutes a valuable therapeutic target for diminishing mitochondrial dysfunction and neuronal injury after a transient ischemic event has occurred.

Current studies, using the acute hippocampal slice model of ischemia, have further examined the progression of changes over several hours after a short episode (8 min) of OGD. We found that, 4-5 h after OGD, mitochondria of CA1 neurons are markedly depolarized and swollen. Spontaneous synaptic activity, assessed as the frequency of spontaneous postsynaptic currents (SPSCs), initially decreases after OGD, but later quickly and markedly increases (~5 fold), before decreasing again to levels below control. Next, we demonstrated that preventing the mitochondrial Zn^{2+} accumulation by MCU inhibition (with ruthenium red [RR]) or by Zn^{2+} chelation after OGD withdrawal substantially attenuated changes in mitochondrial potential ($\Delta\Psi_m$) and synaptic function, and RR largely reversed mitochondrial swelling.

Finally, in test of principle studies using an *in vivo* rat asphyxial cardiac arrest (CA)/resuscitation model, intravenous infusion of RR immediately after resuscitation substantially decreased both the mitochondrial Zn^{2+} accumulation and the mitochondrial and neuronal damage, supporting the possible therapeutic utility of postischemic treatments targeting mitochondrial Zn^{2+} accumulation through the MCU.

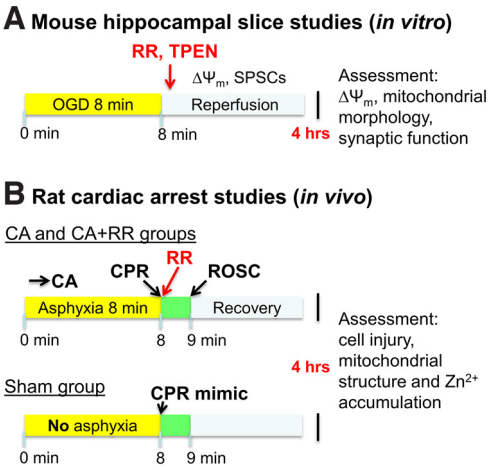

Figure 1. Experimental procedure. ***A***, OGD in brain slices. Schematic show steps of experiment modeling ischemia/reperfusion in acute brain slices. ***B***, *In vivo* CA/CPR experimental procedure. Schematic represents steps of an experiment modeling CA-evoked transient global ischemia in rats. RR was administered to the CA+RR group at the time of CPR. All animals were cannulated, intubated, and attached to ventilator before CA or sham procedure. Chest compressions were performed on sham animals to mimic CPR.

Materials and Methods

Animals

Animal care and experimental procedures were performed according to a protocol approved by University of California Irvine Animal Care and Use Committee. Efforts were made for minimizing animal number and suffering. Both male and female mice from 129S6/SvEvTac strain (Taconic Biosciences; ~ 4 weeks old) were used for *in vitro* experiments, and male Wistar rats (Charles River Laboratories) weighing 300-350 g (8-12 weeks) were used for *in vivo* CA studies.

Preparation of acute hippocampal slices

Coronal hippocampal slices were prepared from ~4-week-old mice as previously described (Medvedeva et al., 2009). Mice were deeply anesthetized with isoflurane and decapitated. The brains were quickly removed and placed in ice-cold solution containing the following (in mM): 220 sucrose, 3 KCl, 1.25 NaH_2PO_4, 6 $MgSO_4$, 26 $NaHCO_3$, 0.2 $CaCl_2$, 10 glucose, and 0.42 ketamine (pH 7.35, 310 mOsm, equilibrated with 95% O_2/5% CO_2). Ketamine was added to preparation solution to decrease NMDA-mediated Ca^{2+} influx caused by cutting trauma. Hippocampal slices (300 µm) were cut using a Leica VT1200 vibratome, with vertical vibration of cutting blade adjusted to be <1 µm to decrease injury. After preparation slices were incubated in ACSF containing the following (in mM): 126 NaCl, 3 KCl, 1.25 NaH_2PO_4, 1 $MgSO_4$, 26 $NaHCO_3$, 2 $CaCl_2$, 10 glucose (pH 7.35, 310 mOsm, equilibrated with 95% O_2/5% CO_2) for 1 h at 34 ± 0.5°C, and then kept at room temperature (20°C-23°C) in oxygenated ACSF. All experiments were performed at 32 ± 0.5°C.

OGD in slices and drug administration

To induce hypoxia-hypoglycemia, ACSF was changed to identical solution without glucose and equilibrated with 95% N_2/5% CO_2. For sublethal (short) ischemic exposures, OGD was terminated (by restoration of oxygenated ACSF containing glucose) after 8 min (Fig. 1*A*). The duration of OGD was determined by our previous experiments with the aim to withdraw OGD before Ca^{2+} deregulation occurs in the majority of CA1 neurons while allowing sufficient time to evoke mitochondrial depolarization (loss of $\Delta\Psi_m$), Zn^{2+} accumulation and delayed (4 h later) mitochondrial dysfunction (Medvedeva et al., 2009, 2017) (see Fig. 3). Since our experiments required use of slices for prolonged periods (up to 7 h), all measurements in OGD subjected slices are compared with results obtained from control slices at approximately the same time after slice preparation.

RR (10 μM) and N,N,N',N'-tetrakis(2-pyridylmethyl)ethane-1,2-diamine (TPEN, 20 μM) were applied 3 min and immediately after the OGD termination, respectively.

Evaluating neuronal visual appearance and fluorescent measurements

To assess changes in cellular morphology slices were placed under the bright field microscope equipped with differential interference contrast (DIC) optics (Olympus) and photographed. All further evaluations were conducted blindly (using coded images), by an investigator not involved in performing experiments. CA1 neuronal diameters, determined as the maximum width of the cell perpendicular to the apical dendrite, were measured using ImageJ software. Only neurons where we can clearly distinguish the cellular membrane were evaluated.

To study changes in mitochondrial function, we assessed $\Delta\Psi_m$. Slices were bath-loaded with the $\Delta\Psi_m$-sensitive indicator, Rhodamine 123 (Rhod123, 26 μM, 30 min, 22°C-24°C). Rhod123 is positively charged and accumulates in negatively charged mitochondria where its fluorescence is quenched. Upon loss of $\Delta\Psi_m$, the indicator is released into the cytoplasm causing increase in fluorescence (Duchen et al., 2003). Rhod123 was excited at 540(25) nm and emitted fluorescence was collected at 605(55) nm. Images were acquired every 15 s. Data are presented as $\Delta F/F_0 = (F - F_0)/F_0$ where F is a current fluorescence intensity and F_0 is baseline fluorescence intensity. Carbonyl cyanide-4-(trifluoromethoxy)phenylhydrazone (FCCP, 2 μM) was applied at indicated time points to evoke full loss of $\Delta\Psi_m$ and consequent increase in Rhod123 fluorescence and, thus, to evaluate the level of $\Delta\Psi_m$ before FCCP application.

Electrophysiological recordings

Slices were placed in a flow-through chamber (RC-27L chamber with plastic slice anchor, Warner Instruments), mounted on the stage of an upright microscope (BX51WI, Olympus) and perfused with oxygenated ACSF at 2 ml/min. To evaluate function of synaptic networks, we recorded SPSCs from CA1 pyramidal neurons, which were patched and held in voltage-clamp configuration at −60 mV using the Axopatch 200A amplifier. For evaluation of the resting membrane potential (MP) and action potential (AP) threshold, we used current-clamp configuration. Patch pipettes used for voltage clamp (5 MΩ resistance when filled with pipette solution) and current clamp (8-10 MΩ) were pulled from borosilicate glass with filament (WPI) on a P-97 micropipette puller (Sutter Instruments). The pipette solution for voltage- and current-clamp recordings contained the following (in mM): 125 K-gluconate, 10 KCl, 3 Mg-ATP, 1 $MgCl_2$, 10 HEPES, pH 7.25 with KOH, 290 mOsm. SPSCs were recorded from neurons in sham slices (not treated with OGD) and at different time points between 1 and 5 h after OGD withdrawal. APs were recorded in sham slices and at ~2.5 h after OGD.

Antibody labeling and confocal microscopy

Hippocampal slices (300 μm) were subjected to OGD for 8 min, "perfused" in ACSF at 32°C for 30 min, then incubated at room temperature for another 3.5 h and fixed with 4% PFA. RR (10 μM) was added to some slices 3 min after OGD termination for 15 min. Thin (30 μm) sections were cut using a microtome cryostat (Thermo Fisher Scientific) and stained with primary antibodies against the mitochondrial outer membrane protein TOM20 (1:200, Santa Cruz Biotechnology) and secondary anti-rabbit fluorescent antibodies (1:200, DyLight 488, Jackson ImmunoResearch Laboratories). To visualize mitochondria, the sections were imaged using an inverted stage FV3000 confocal laser scanning microscope (Olympus) with high-speed resonance scanner, IX3-ZDC2 Z-drift compensator and 40× silicone oil objective (UPLSAPO40XS, NA = 1.25, WD = 0.3 mm). A 488 nm diode laser was used for excitation and a high-sensitivity cooled GaAsP PMT was used for detection of signal.

An analysis of mitochondria size and shape was performed using ImageJ software as previously described (Medvedeva et al., 2017). Images were adjusted to provide optimal discrimination of mitochondria edges from background. We selected the cells that showed clearly evident mitochondria in the perinuclear regions in a sharp focus, and only the mitochondria that are aligned with their long axes parallel to the nuclear membrane were chosen. Measures of long axes, parallel to, and short axes, perpendicular to nuclear membranes were obtained on all clearly demarcated mitochondria adjacent to and surrounding the nuclear circumference. Average parameters were determined for mitochondria within each independent slice experiment, and presented are average values from 4-5 slices for each condition.

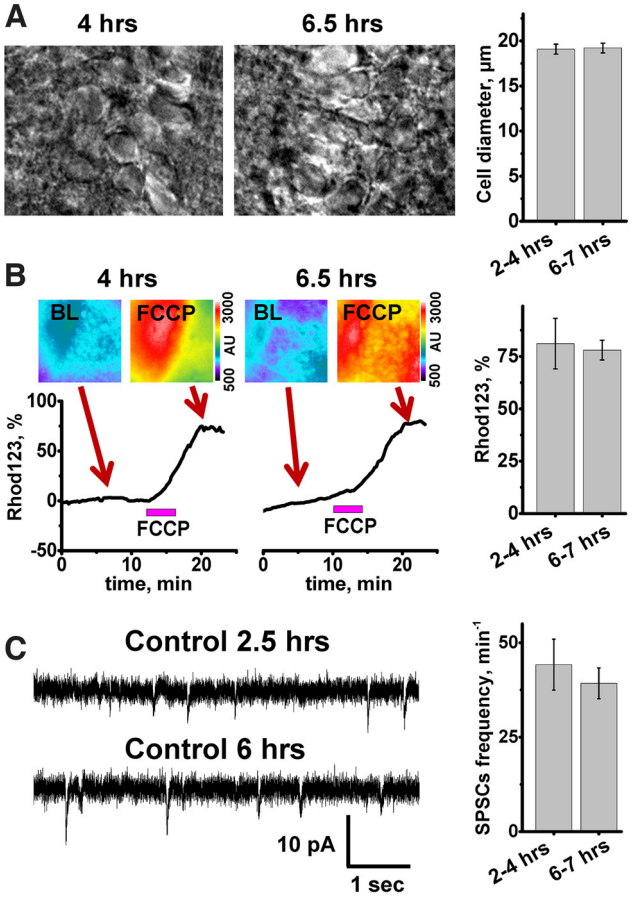

Figure 2. Visual neuronal appearance, mitochondrial potential, and spontaneous synaptic activity do not change during 7 h after slice preparation. ***A***, Left, middle, Bright field images of CA1 region of representative slices at indicated time after slice preparation. Right, Bar graphs represent average diameter of CA1 neuronal somata. No differences were found between pyramidal neuron diameters at 2-4 h (28 slices evaluated, 19.1 ± 0.6 μm) and at 6-7 h (7 slices, 19.2 ± 0.5 μm, $p = 0.9$, *t* test). ***B***, Assessment of $\Delta\Psi_m$. Brain slices were loaded with Rhod123, and FCCP (2 μM) was applied after 10-20 min of baseline (BL) recording. Top, Pseudocolor Rhod123 fluorescent images of slices before (BL) and after FCCP application. Bottom, Traces represent Rhod123 $\Delta F/F_0$ changes. Arrows indicate the time points at which fluorescent images were taken. Right, Bar graph represents average Rhod123 $\Delta F/F_0$ (±SE) after FCCP application 2-4 h (81.1 ± 12%, $n = 11$) and 6-7 h (78 ± 4.5%, $n = 11$, $p = 0.72$, *t* test) after slice preparation. ***C***, SPSCs recorded from CA1 neurons. Left, Representative recordings of SPSCs 2.5 h (top) and 6 h (bottom) after slice preparation. Right, Bar graph represents average SPSC frequency (±SE) (44.2 ± 6.7 min^{-1}, $n = 10$ in 2-4 h group, and 39.7 ± 3.6 min^{-1}, $n = 8$ at 6-7 h after slice preparation, $p = 0.59$, *t* test).

CA/cardiopulmonary resuscitation (CPR) and RR administration

This study utilizes an asphyxial CA+CPR model similar to previously described (Crouzet et al., 2016, 2020; Kang et al., 2017). Rats were calorically restricted to 25% of normal food intake 14 h before CA (Azadian et al., 2020). Shortly before the experiment, rats were intubated using a 14-gauge endotracheal tube (B. Braun Melsungen AG), connected to a TOPO mechanical ventilator (Kent Scientific) and isoflurane vaporizer for delivery of 2% isoflurane and 50% O_2/50% N_2 gas mixture during surgical preparation. Femoral artery and vein cannulation allowed monitoring of blood pressure and heart rate, and

administration of intravenous medication. Invasive arterial blood pressure was measured continuously using a transducer (CWE).

After surgical preparation, CA experiments began with reducing the isoflurane level to 1%-1.5% to prepare for anesthesia washout. The inhaled gas was switched to 100% O_2 for 2 min, after which the isoflurane was stopped to wash out anesthesia for 3 min. When the isoflurane was stopped, the inlet was also disconnected from oxygen to allow room air to be mechanically delivered to the rat. Additionally, neuromuscular blockade was also initiated at this time with injection of 1 ml of intravenous vecuronium (2 mg/kg) with 1 ml of heparinized saline. After these 3 min of isoflurane washout, asphyxial CA was induced by turning the ventilator off and clamping the ventilator tubing. CA time was defined as systolic blood pressure $<$30 mmHg and pulse pressure of $\leq$10 mmHg. Baseline arterial blood gas measurements were obtained within 30 min before initiation of asphyxia. Duration of asphyxia was 8 min. In the last min of asphyxia, as the ventilator is being reconnected and turned on, epinephrine (0.01 mg/kg) and bicarbonate (140 mg/kg) are given ahead of CPR to stimulate the sympathetic nervous system and manage acidosis, respectively. CPR (manual sternal compressions at 180-240 per min) was performed after 8 min of asphyxia and continued until return of spontaneous circulation (ROSC). Our study used 3 groups of animals: (1) sham treatment group (control, this group was subjected to all experimental procedure without asphyxia); (2) rats subjected to CA without treatment; and (3) rats subjected to CA with MCU blocker RR administered intravenously at the time of CPR to reach the brain with ROSC (Fig. 1*B*), as we have demonstrated with other drugs administered during the CPR phase (Kang et al., 2017). After obtaining post-CA arterial blood gas measurements 10 min after ROSC, vessels were decannulated and rats were extubated within the following hour.

Histochemistry and electron microscopy

Cardiac perfusion and preparation for Timm's labeling. To detect neuronal injury and reactive Zn^{2+} accumulation at the intracellular sites, we used a modification of the Timm's sulfide silver method in combination with histochemistry (Danscher and Zimmer, 1978; De Biasi and Bendotti, 1998). Four hours after CPR, animals were anesthetized with isoflurane, and perfused transcardially with 200 ml of PBS for 2 min, followed by 500 ml of Millonig's buffer (containing 0.002% $CaCl_2$, 1.6% NaH_2PO_4, and 0.4% NaOH; pH 7.3), also containing 0.2% Na_2S, 4% PFA, and 1% glutaraldehyde over the next 20 min to precipitate Zn^{2+}. After perfusion, the brains were postfixed using 2% PFA/2.5% glutaraldehyde/0.2% Na_2S at 4°C overnight, and 50 and 80 μm slices were cut using vibratome.

Timm's labeling. To analyze Zn^{2+} accumulation in mitochondria, we performed

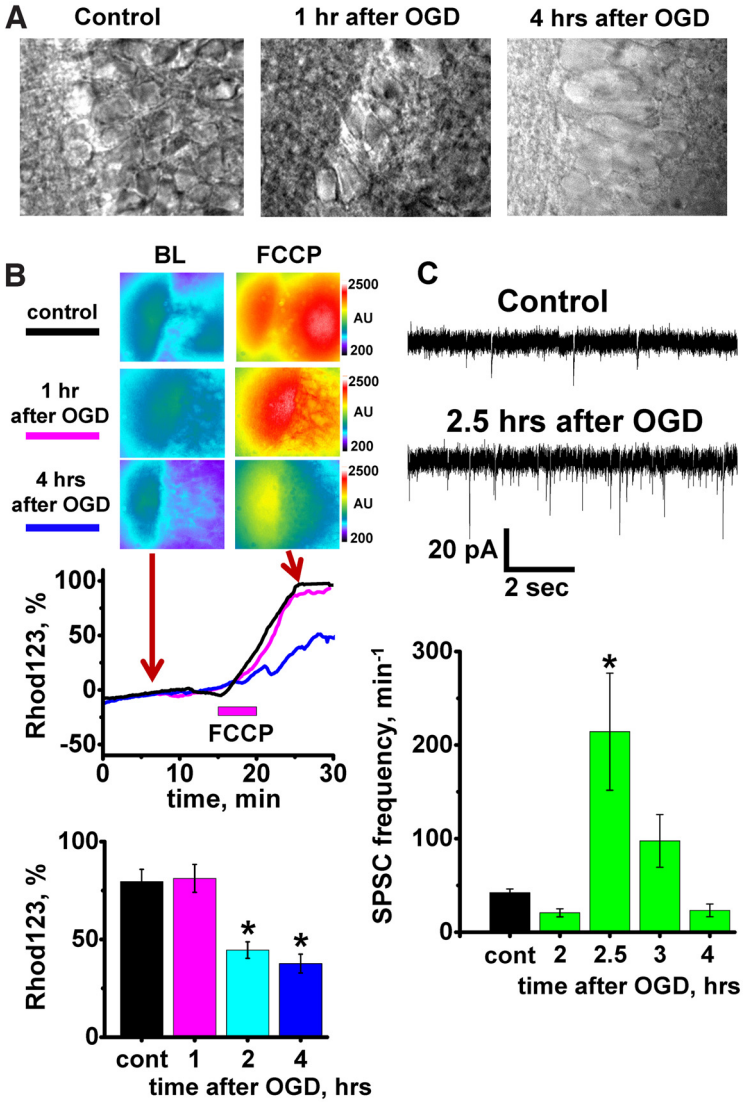

Figure 3. Short OGD causes delayed neuronal swelling, persistent mitochondrial dysfunction, and changes in spontaneous synaptic activity in CA1 neurons. ***A***, Bright field images of CA1 neurons in control slice, and in slices 1 and 4 h after OGD termination. Note similar appearance of neurons in control slice and 1 h after OGD. After longer period (4 h), neurons were markedly swollen (average diameter of CA1 neurons was 32.4 ± 1.0, $n = 8$ slices 4 h after OGD vs 19.2 ± 0.5 μm, $n = 34$ slices in control, $p < 0.001$, *t* test). ***B***, $\Delta\Psi_m$ changes after OGD in CA1. Slices were subjected to sham treatment or to OGD and later loaded with Rhod123. FCCP (2 μM) was applied to sham-treated slices (control) or at indicated times after OGD to evoke loss of $\Delta\Psi_m$. Top, Fluorescent images were taken before (BL) and after FCCP application. Arrows indicate time points at which fluorescent images were taken. Traces represent Rhod123 $\Delta F/F_0$ changes in the same slices (black - control; magenta - 1 h; blue - 4 h after OGD withdrawal). Bottom, Bar graph represents average Rhod123 $\Delta F/F_0$ changes (±SE) in control slices and after OGD at indicated times. (Control 79.5 ± 6.3%, $n = 22$ evaluated slices; 1 h 81.2 ± 7.2%, $n = 10$; 2 h 44.6 ± 4.2%, $n = 13$; and 4 h after OGD 37.7 ± 4.8%, $n = 9$). Note the significant decrease in Rhod123 $\Delta F/F_0$ 2 and 4 h after OGD ($p < 0.01$ compared with 1 h after OGD or corresponding control, two-way ANOVA Bonferroni test). *$p < 0.01$ compared with control. While we used 3 separate control groups for statistical analyses, we found no difference between the controls ($p = 0.93$, one-way ANOVA); thus, bar graph represents an average fluorescence value of all control slices. ***C***, SPSC recordings from CA1 neurons. Top, Traces demonstrate SPSCs recorded from representative neurons in control slices and 2.5 h after OGD withdrawal. Bottom, Bar graph represents average frequency of SPSCs (±SE) in CA1 neurons in control (42.2 ± 4.0, $n = 18$, bar shows average data for all control slices, as there were no differences between controls at different time points, $p = 0.86$, one-way ANOVA) and at indicated time points after OGD (24.2 ± 3.4 min^{-1} after 2 h, $n = 11$; 214.3 ± 62.6 min^{-1} at 2.5 h, $n = 8$; 97.6 ± 28.2 min^{-1} at 3 h, $n = 7$; and 23.3 ± 6.8 min^{-1} at 4 h, $n = 10$). Note the abrupt increase in SPSC frequency at 2.5 h after OGD ($p < 0.001$, compared with other time points or control, two-way ANOVA Bonferroni test). *$p < 0.001$ versus control.

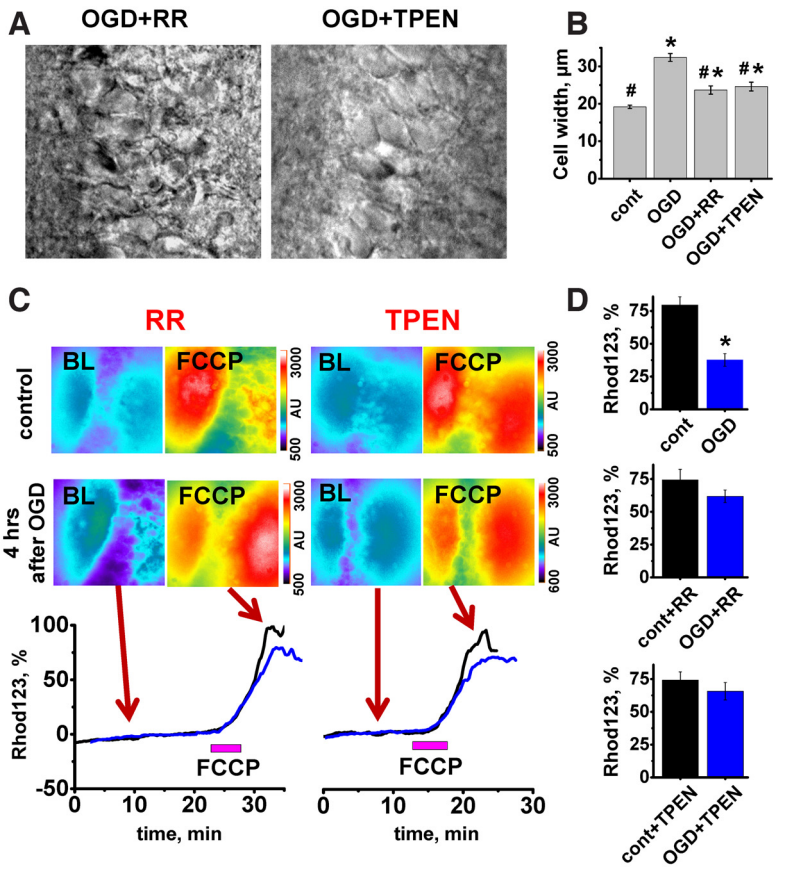

Figure 4. MCU inhibition or Zn^{2+} chelation after an OGD episode attenuates delayed neuronal swelling and mitochondrial depolarization. ***A***, Representative bright field images of CA1 neurons 4 h after the short OGD episode in slices treated with RR or TPEN. ***B***, OGD-induced neuronal swelling was attenuated by RR or TPEN. Bar graph represents average diameter of CA1 neurons in control and 4 h after OGD with or without treatments (control 19.2 ± 0.5 μm, $n = 34$ slices; OGD 32.4 ± 1.0, $n = 8$ slices, $p < 0.001$ vs control; OGD+RR 23.7 ± 1.1, $n = 17$ slices, $p < 0.001$ vs OGD alone or control; OGD+TPEN 24.6 ± 1.2, $n = 19$ slices, $p < 0.001$ vs OGD alone or control, one-way ANOVA Bonferroni test). *$p < 0.001$ compared with control. #$p < 0.001$ versus OGD. As we did not find difference in cell diameter between control nontreated and TPEN or RR-treated slices ($p = 0.7$, one-way ANOVA), the control bar represents grouped data. ***C***, OGD-evoked changes in $\Delta\Psi_m$ were attenuated by RR or TPEN. Top, Fluorescent images of Rhod123-loaded slices recorded before (BL) and after FCCP application (2 μM) in control slices and 4 h after OGD episode. Left, Slices, both control and subjected to OGD, were treated with RR (10 μM) as described. Right, Slices treated with TPEN (20 μM). Bottom, Traces below demonstrate FCCP-evoked Rhod123 $\Delta F/F_0$ changes. Black traces represent changes in control slices. Blue traces represent slices subjected to OGD, 4 h after OGD episode. Arrows indicate time points at which fluorescent images were taken. ***D***, Bar graphs represent average Rhod123 $\Delta F/F_0$ increase (±SE) after FCCP application (top, no treatment: control 79.5 ± 6.3%, $n = 22$, OGD 37.7 ± 4.8%, $n = 9$, $p < 0.001$; middle, treated with RR: control+RR 74.3 ± 8.1%, $n = 12$; OGD+RR 61.8 ± 4.8%, $n = 12$, $p = 0.2$; bottom, TPEN: control+TPEN 74.2 ± 6.3%, $n = 12$; OGD+TPEN 65.8 ± 6.7%, $n = 12$, $p = 0.37$, t test). *$p < 0.001$ versus control. Both treatments provide considerably better-preserved mitochondrial potential compared with OGD alone ($p < 0.01$ for both TPEN and RR). The significance of effect of treatment on OGD-evoked loss of $\Delta\Psi_m$ was assessed with ANOVA linear contrast.

Timm's labeling, which inserts metallic silver precipitates at sites of labile (loosely bound or reactive) Zn^{2+} accumulation. For Timm's staining, 80 μm slices were incubated in the dark in a solution containing 1 part of 1 M $AgNO_3$ solution, 20 parts solution containing 2% hydroquinone and 5% citric acid in water, and 100 parts of solution containing 30% gum Arabic in water. Development was performed in the dark, was monitored by periodic evaluations under low light, and was terminated by washing in water. Stained slices were placed into PBS and processed for electron microscopy.

Electron microscopy. For transmission electron microscopy analysis, we used ultrathin sections (~1 μm thickness) prepared largely as previously described (Park et al., 2016) with small modifications. The sections were rinsed in PBS and postfixed with 1% osmium tetroxide in PBS for 1 h, then dehydrated in increasing serial dilutions of ethanol (70%, 85%, 95%, and 100%), placed into intermediate solvent propylene oxide (2 times for 10 min), and incubated in 1:1 mixture of propylene oxide/Spurr's resin for 1 h. Finally, slices were embedded in Spurr's resin overnight. Ultrathin sections (~70 nm thickness) were cut using a Leica Ultracut UCT ultramicrotome (Leica) mounted on 150 mesh copper grids, stained with lead citrate, and viewed using a JEOL 1400 electron microscope (JEOL). Images were captured using a Gatan digital camera (Gatan).

VAF/toluidine blue staining. To assess neuronal injury, after perfusion, tissue fixation and slice preparation as described, 30 μm sections were stained with vanadium acid fuchsin (VAF) or toluidine blue (TB) largely as previously described (Victorov et al., 2000). Slices were stained with VAF for 1-2 min, washed with PBS, incubated in 0.01% borax solution for 20-30 s, and rinsed in distilled water. Finally, brain slices were cleared by acetate buffer (pH 3.3) for 30 s and rinsed with distilled water. Another group of slices was stained with 0.025% toluidine blue for 20-30 s. Stained slices were assessed and photographed using light microscopy. Cell counts of injured versus healthy neurons were conducted blindly by an investigator not involved in performing the experiments.

Reagents

Rhod123 was obtained from Invitrogen. N,N,N',N'-tetrakis(2-pyridylmethyl)ethylenediamine, RR, and ketamine were obtained from Sigma. TOM20 antibodies were obtained from Santa Cruz Biotechnology, and DyLight 488 antibodies were obtained from Jackson ImmunoResearch Laboratories. All other reagents were purchased from Thermo Fisher Scientific.

Statistics and data analysis

All comparisons reflect sets of data substantially interleaved in time. Evaluations of mitochondrial and neuronal health and morphology were performed blindly using coded images.

For comparisons between 2 groups, statistical differences were assessed using two-sample t tests. To evaluate differences between >2 sets of data with one changing factor (including controls at different time points after slice preparation or controls with/without treatment), we used one-way ANOVA with Bonferroni test. To evaluate time-dependent changes in $\Delta\Psi_m$ and SPSC frequency caused by OGD, we used two-way ANOVA Bonferroni test with interactions where the first factor was time and the second one was OGD. For these tests, we used control groups of slices at the same time points after slice preparation as slices from OGD-treated groups that were subjected to identical manipulations but without OGD. All tests described above were performed using Origin 9.1 (OriginLab). To evaluate the significance of protection provided by pharmacological interventions (RR or TPEN, assessed as difference between measurements in slices subjected to OGD and control slices, vs difference between OGD+treatment and control+treatment), we used ANOVA linear contrast (coded with R language). The R code used for calculating the contrasts is available on request.

In vitro *experiments.* Since our preliminary experiments did not find any differences of investigated parameters between slices of female and male animals, all further analysis included slices from animals of both sexes. We performed one or two slice experiments per animal per condition. For electrophysiological recordings, one neuron was examined per slice. All comparisons were made based on $n \geq 6$. For analysis of mitochondrial morphology, measured parameters were averaged for each

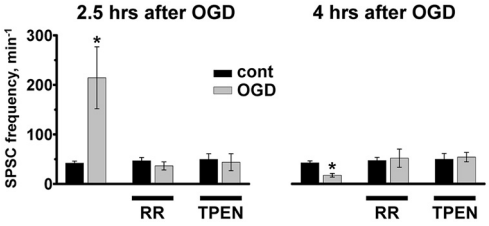

Figure 5. MCU inhibition or Zn^{2+} chelation attenuates changes in synaptic activity after sublethal OGD. Left, Treatment with either RR or TPEN shortly after OGD withdrawal reversed increase in SPSC frequency observed 2.5 h after OGD (SPSC frequency after OGD without treatment was $214.3 \pm 62.6\ min^{-1}$, $n = 8$ vs 42.2 ± 4.0, $n = 18$ in control, $p < 0.001$; after OGD+RR, $36.5 \pm 8.2\ min^{-1}$, $n = 7$ vs 46.8 ± 6.6, $n = 9$ in control+RR, $p = 0.35$; after OGD+TPEN, $43.9 \pm 17.1\ min^{-1}$, $n = 7$ vs 49.5 ± 11.6, $n = 9$ in control+TPEN, $p = 0.78$, *t* test). *$p < 0.001$ compared with control. Right, Treatment with RR or TPEN prevents silencing of SPSCs 4 h after OGD (SPSC frequency after OGD was: $17.3 \pm 3.6\ min^{-1}$, $n = 9$ vs 42.2 ± 4.0, $n = 18$ in control, $p < 0.001$; after OGD+RR, $51.6 \pm 18.3\ min^{-1}$, $n = 6$ vs 46.8 ± 6.6, $n = 9$ in control+RR, $p = 0.78$; after OGD+TPEN, $58 \pm 7.5\ min^{-1}$, $n = 8$ vs 49.5 ± 11.6, $n = 9$ in control+TPEN, $p = 0.56$, *t* test). *$p < 0.001$ compared with control. Bar graphs represent average frequency of SPSCs (±SE). Notably, both treatments largely eliminated the OGD-evoked increase in SPSC frequency at 2.5 h ($p < 0.01$ for RR and $p < 0.01$ for TPEN compared with OGD without treatment) and the decrease in SPSC frequency at 4 h after OGD ($p < 0.05$ for both RR and TPEN, significance of differences was evaluated using ANOVA linear contrast).

neuron, only neurons with $n \geq 3$ clearly recognizable mitochondria were used, and data averaged per each slice experiment.

In vivo *experiments.* To analyze neuronal health (using TB or VAF staining), we evaluated 3-5 sections per animal with 50-100 cells examined per each section. To evaluate mitochondrial shape, structural changes, and Zn^{2+} accumulation, >120 mitochondria from ≥9 sections (≥3/animal) were evaluated per condition. All data obtained in *in vivo* experiments were averaged per each animal.

Results

Dynamic changes of CA1 neuronal visual appearance, mitochondrial potential, and synaptic function after OGD

Our recent observations of prolonged Zn^{2+} accumulation in mitochondria of CA1 neurons after ischemia (Medvedeva et al., 2017; Yin et al., 2019) led to the hypothesis that this Zn^{2+} accumulation could be a key trigger of delayed ischemic injury. Indeed, the delayed injury of CA1 neurons is characterized by mitochondrial swelling and release of cytochrome C (Nakatsuka et al., 1999; Sugawara et al., 1999), effects that are compatible with observations of Zn^{2+} triggered mitochondrial permeability transition pore (mPTP) opening and cytochrome C release (Wudarczyk et al., 1999; D. Jiang et al., 2001; Calderone et al., 2004; Gazaryan et al., 2007). To test our hypothesis, we developed a hippocampal slice model of "sublethal" ischemia and reperfusion, which does not cause acute cell death but evokes a sequence of events likely leading to delayed cell injury. Slices were subjected to short (8 min) episodes of OGD (or sham wash in oxygenated media for control) and were monitored over the subsequent 4-5 h to assess delayed pathologic changes. However, since these experiments have prolonged durations (~6 h), we first sought to confirm neuronal viability for 6-7 h after slice preparation. Several parameters were evaluated: neuronal visual appearance (using DIC optics), stability of $\Delta\Psi_m$, which reflects mitochondrial function, and spontaneous synaptic activity, to assess function of synaptic networks. After examination of DIC images of CA1 regions from 2 groups of slices (those at 2-4 h after preparation and at 6-7 h), we found no difference in cell appearance and neuronal diameter between groups (Fig. 2*A*). Of note, ~10% of slices in both groups had mild neuronal swelling probably because of damage from preparation.

$\Delta\Psi_m$ was monitored using the fluorescent indicator, Rhod123. This positively charged indicator is sequestered by negatively charged mitochondria, where its fluorescence is quenched, and the accumulated amount is proportional to $\Delta\Psi_m$. Application of the mitochondrial uncoupler FCCP (2 μM, 5 min), which dissipates the proton gradient across the mitochondrial inner membrane, results in loss of $\Delta\Psi_m$ and consequent release of Rhod123 into the cytosol and a corresponding increase in fluorescence (ΔF). This ΔF is indicative of the $\Delta\Psi_m$ before FCCP exposure. We found that untreated slices reliably maintained their $\Delta\Psi_m$ for at least 6-7 h (Fig. 2*B*).

To evaluate synaptic function, SPSCs were recorded over time from individual CA1 neurons using patch-clamp technique in voltage-clamp mode (at −60 mV). We found that SPSCs occurred at a stable frequency for up to 7 h after slice preparation (Fig. 2*C*). In this study, we monitored only the inward excitatory synaptic currents since the reversal potential for Cl^- was −61 mV; thus, the inhibitory outward currents were indistinguishable from noise.

Short OGD caused extensive changes in all monitored parameters. While neurons appeared intact and visually not different from control on images obtained 1, 2, and 3 h after OGD, this quickly changed from 3 to 4 h; and by the 4 h time point, most CA1 neurons in all slices became severely swollen (Fig. 3*A*) with considerably increased diameters (Fig. 4*B*).

To evaluate dynamic changes in $\Delta\Psi_m$, FCCP (2 μM) was applied to Rhod123-loaded slices 1, 2, and 4-5 h after OGD termination. Our past studies demonstrated that, during OGD $\Delta\Psi_m$ declines rapidly beginning a few minutes after the start of the OGD episode, but recovers relatively quickly upon reperfusion (Medvedeva et al., 2009, 2017). Here we found that, similar to previous observations, $\Delta\Psi_m$ initially recovered to pre-OGD level. However, 2 h after OGD, we detected a substantial drop of $\Delta\Psi_m$, which persists at 4-5 h (Fig. 3*B*), when experiments were terminated.

Since changes in both synaptic structure and function were documented previously in cortex and hippocampus after *in vivo* and *in vitro* ischemia (Jourdain et al., 2002; Crepel et al., 2003; Ai and Baker, 2006; Kovalenko et al., 2006; Radenovic et al., 2011; Neumann et al., 2013), we next sought to determine the dynamic effect of OGD/reperfusion on function of synaptic circuitry in slice. The frequency of SPSCs was evaluated in CA1 pyramidal neurons at multiple time points during 4 h after OGD. In contrast to the stable SPSC frequency noted in control slices, after short OGD, it initially dropped but later increased to ~5-fold greater than basal rates at ~2.5 h after OGD withdrawal. After peaking between 2 and 3 h, the SPSC frequency declined again to substantially below baseline level by 4 h (Fig. 3*C*).

We further questioned whether the abrupt increase in synaptic activity after OGD is facilitated by changes in intrinsic neuronal physiology of CA1 or CA3 neurons. To measure the physiological cell properties, we evaluated the resting MP and the threshold for AP generation in CA1 and CA3 neurons in control slices and 2.5 h after OGD. Single APs were elicited by injecting brief suprathreshold depolarizing current pulses into patched neurons. We did not find evidence of differences in MP or AP threshold 2.5 h after OGD compared with control in either CA1 or CA3 neurons (CA1: MP was -62 ± 0.6 mV, $n = 9$ in control and -61 ± 1.3 mV

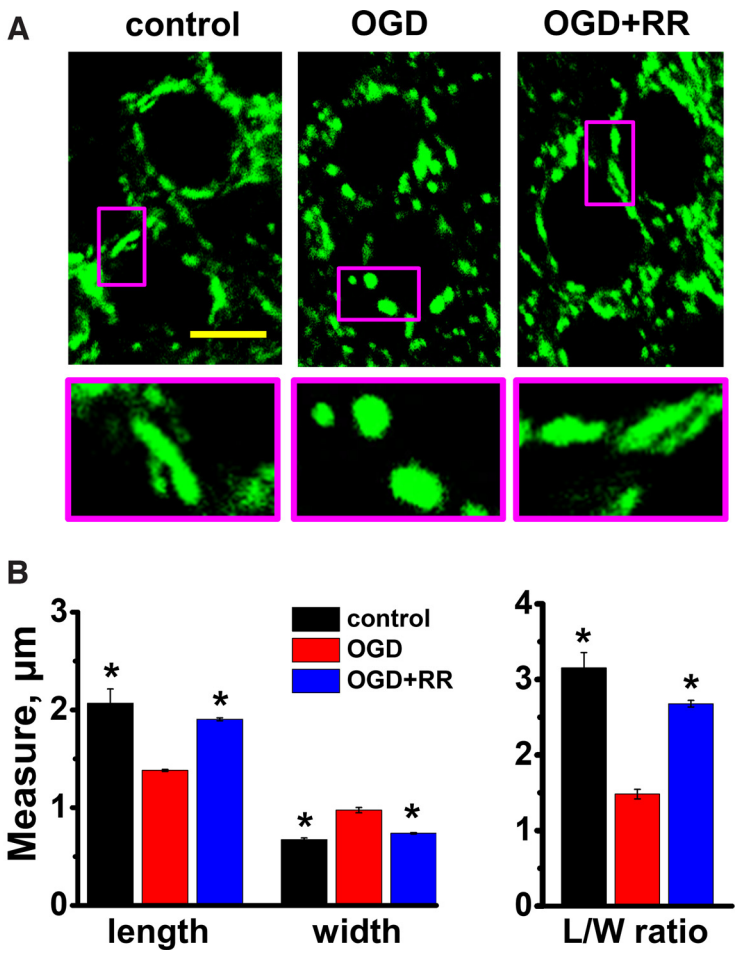

Figure 6. Mitochondrial swelling after OGD in CA1 pyramidal neurons is attenuated by MCU blockade. Brain slices were subjected to sham wash in oxygenated medium (control) or to 8 min OGD either alone or with RR (10 μM, applied 3 min after OGD withdrawal for 15 min). Four hours after OGD, slices were fixed (with 4% PFA) and stained with TOM-20 antibody. ***A***, Appearance of mitochondria in CA1 neurons. Representative confocal images show TOM-20-labeled mitochondria. Scale bar, 10 μm. Enlarged images (bottom) of regions indicated on top panel show representative mitochondria at high magnifications. OGD caused fragmentation and a "rounding up" of mitochondria, with decrease in length and increase in width; this change was attenuated by delayed treatment with RR. ***B***, Quantitative measurements. Left, Bar graphs represent average mitochondrial measurements (length and width; obtained using ImageJ software) of independently treated hippocampal slices after the indicated treatment. Each bar comprises mean from $n \geq 4$ slices for each condition (>100 mitochondria were measured per condition from 34 neurons in control, 48 neurons after OGD, and 51 neuron in slices treated with OGD followed by RR). Length (in μm): control 2.1 ± 0.1; OGD 1.4 ± 0.01; OGD+RR 1.9 ± 0.01. Width (in μm): control 0.7 ± 0.02; OGD 1.0 ± 0.03; OGD+RR 0.7 ± 0.01. Right, Bar graphs represent mean L/W ratios observed after each treatment (based on the same data; control 3.2 ± 0.2; OGD 1.5 ± 0.06; OGD+RR 2.7 ± 0.04). *$p < 0.01$ versus OGD alone (one-way ANOVA).

after OGD, $n = 9$, $p = 0.6$; AP threshold was −54 ± 1.4 mV, $n = 9$ in control and −54 ± 1.7 mV, $n = 9$ after OGD, $p = 1$. CA3: MP in control cells was −62.2 ± 1 mV, $n = 9$ and −62.4 ± 1 mV after OGD, $n = 9$, $p = 0.9$; AP threshold was −51 ± 1.3 mV in control neurons, $n = 9$ and −51 ± 0.7 after OGD, $n = 9$, $p = 1$; all comparisons by t test). As the increased SPSC frequency seen in CA1 neurons after OGD did not appear to be explained by increased intrinsic excitability of either CA3 or CA1 neurons, we suggest that the SPSC frequency increase may be best explained as a manifestation of forms of LTP of the CA3-CA1 synapses as has been previously observed to occur after transient brain ischemia (Jourdain et al., 2002; Crepel et al., 2003; Ai and Baker, 2006).

Mitochondrial Zn^{2+} uptake after sublethal OGD contributes to delayed changes in CA1 neurons

To investigate the contribution of prolonged mitochondrial Zn^{2+} accumulation after OGD to observed morphologic and functional alterations, we blocked the primary route for Zn^{2+} uptake into mitochondria, the MCU (Malaiyandi et al., 2005; Medvedeva et al., 2017; Ji et al., 2020), with RR (10 μM applied ~3 min after OGD withdrawal for 15 min). Treatment with RR noticeably improved the appearance of CA1 pyramidal neurons 4 h after OGD (Fig. 4*A*, compare with Fig. 3*A*) considerably diminishing their swelling (measured as changes in cell diameters; Fig. 4*B*). RR treatment also markedly attenuated the loss of $\Delta\Psi_m$ 4-5 h after OGD withdrawal (Fig. 4*C*,*D*).

Since the MCU is also the route for Ca^{2+} accumulation into mitochondria, to study whether the observed beneficial effects are caused specifically by Zn^{2+}, in another set of experiments, we tested the membrane permeable specific Zn^{2+} chelator TPEN (20 μM, applied immediately after OGD for 20 min). Similar to findings with RR, treatment with TPEN markedly decreased the swelling of CA1 neurons (Fig. 4*B*). Loss of $\Delta\Psi_m$ observed 4-5 h after the ischemic episode was also considerably attenuated (Fig. 4*C*,*D*).

Next, we questioned whether alterations in synaptic function observed after OGD are dependent on mitochondrial Zn^{2+} accumulation. We found that treatments with RR or TPEN reversed OGD evoked changes in synaptic activity, both preventing the aberrant burst of SPSCs at 2-3 h and reversing the synaptic quieting 4-5 h after OGD (Fig. 5).

Mitochondrial swelling after OGD in CA1 pyramidal neurons is attenuated by MCU inhibition

Our recent study demonstrated a strong association between mitochondrial Zn^{2+} accumulation, mitochondrial swelling, and mitochondrial structural changes after transient global ischemia in a rat model of CA (Yin et al., 2019). Current studies used confocal microscopy to investigate effects of mitochondrial Zn^{2+} accumulation after OGD/reperfusion on mitochondrial morphology in acute slices. As above, slices were exposed to sham wash in oxygenated media (control) or to an 8 min episode of OGD and reperfusion, either alone or with RR applied 3 min after the end of the OGD for 15 min. Four hours after OGD, slices were fixed with PFA and stained with antibodies for the mitochondrial outer membrane protein, TOM20. Confocal (1000×) images were obtained from the CA1 pyramidal layer (Fig. 6*A*). Mitochondrial morphologic parameters were analyzed as described previously (Medvedeva et al., 2017). We found that OGD caused a noticeable fragmentation and swelling of the mitochondria (Fig. 6*A*) with substantial decreases in their lengths, increases in their widths, and considerably decreased length/width (L/W) ratios (control 3.2 ± 0.20, OGD 1.5 ± 0.06, Fig. 6*B*). This mitochondrial swelling correlates with the persistent mitochondrial depolarization noted

above. We found that application of RR substantially attenuated the observed mitochondrial swelling (Fig. 6*A*,*B*, L/W ratio 2.7 ± 0.04).

MCU inhibition decreases CA1 neuronal injury after global ischemia in rats

Finally, we tested whether inhibiting the MCU after an episode of global ischemia improves neuronal recovery *in vivo*. Rats were subjected to sham treatment, to asphyxial CA followed by resuscitation (CPR), or to CA/CPR followed by intravenous injection of RR (2.5 mg/kg) (Fig. 1). After 4 h of recovery, rats were perfused, brains isolated and processed for histologic analysis (see Materials and Methods).

To evaluate overall injury of CA1 pyramidal neurons, brain sections were stained with TB to evaluate neuronal morphology or labeled using a modified vanadium acid fuchsin procedure which identifies acidophilic neurons (VAF staining). Sections were then blindly examined using light microscopy, and each identifiable neuron was rated as healthy or injured. Healthy cells in TB-stained slices (Fig. 7*A*, yellow arrows) displayed distinct nonstained round nuclei surrounded by TB-stained cytoplasm, while injured neurons (shown with red arrows) show TB staining in nuclei, cytoplasm, and dendrites. Purple colored VAF labeling in the cytoplasm, which is nominal in healthy neurons, indicates neurons with early moderate injury (Fig. 7*B*, red arrows). We found that, compared with sham treatment, global ischemia caused distinct injury to CA1 pyramidal neurons, similar to that observed in our recent study (Yin et al., 2019). Treatment with RR substantially preserved neuronal morphology and considerably decreased injury (Fig. 7).

CA-induced mitochondrial structural disruption and Zn^{2+} accumulation are attenuated by RR

To investigate effects of global brain ischemia on mitochondria, further studies used transmission electron microscopy techniques to examine mitochondrial ultrastructure. Since somata of CA1 neurons can be identified by their characteristic nuclei, to examine mitochondria in these neurons, we obtained high-magnification transmission electron microscopy images adjacent to nuclei showing mitochondria in perinuclear and proximal dendritic regions. A majority of mitochondria in slices from sham-treated animals appeared intact and healthy. They were usually elongated with visible distinct cristae structure and an intact double membrane (Fig. 8*A*, left). A minority of mitochondria (~30%) had mild injury, with rounder shape, suggesting moderate swelling, and some disruption of their cristae structure (this injury probably was caused by the brain perfusion procedure). After ischemia, the number of injured mitochondria increased greatly; and similar to our previous observations (Yin et al., 2019), a large number (~75%) showed varying degrees of damage 4 h after CA/CPR (Fig. 8*A*, middle, *B*). However, blocking the MCU with RR immediately after CPR substantially decreased the mitochondrial structural damage (Fig. 8*A*, right, *B*).

Since our prior study (Yin et al., 2019) found that mitochondrial injury after ischemia strongly correlates with persistent excessive mitochondrial Zn^{2+} accumulation, we also analyzed Zn^{2+} buildup in mitochondria in the current study. As in our previous study, reactive Zn^{2+} was visualized by Timm's sulfide silver labeling. This stain appears to be quite specific for Zn^{2+}, and was found to be virtually absent in mice lacking the vesicular Zn^{2+} transporter, ZnT3 (Cole et al., 1999). Similar to our recent study, most (>90%) damaged mitochondria (Fig. 8*C*, left), and only a small subset of healthy-appearing mitochondria (Fig. 8*C*,

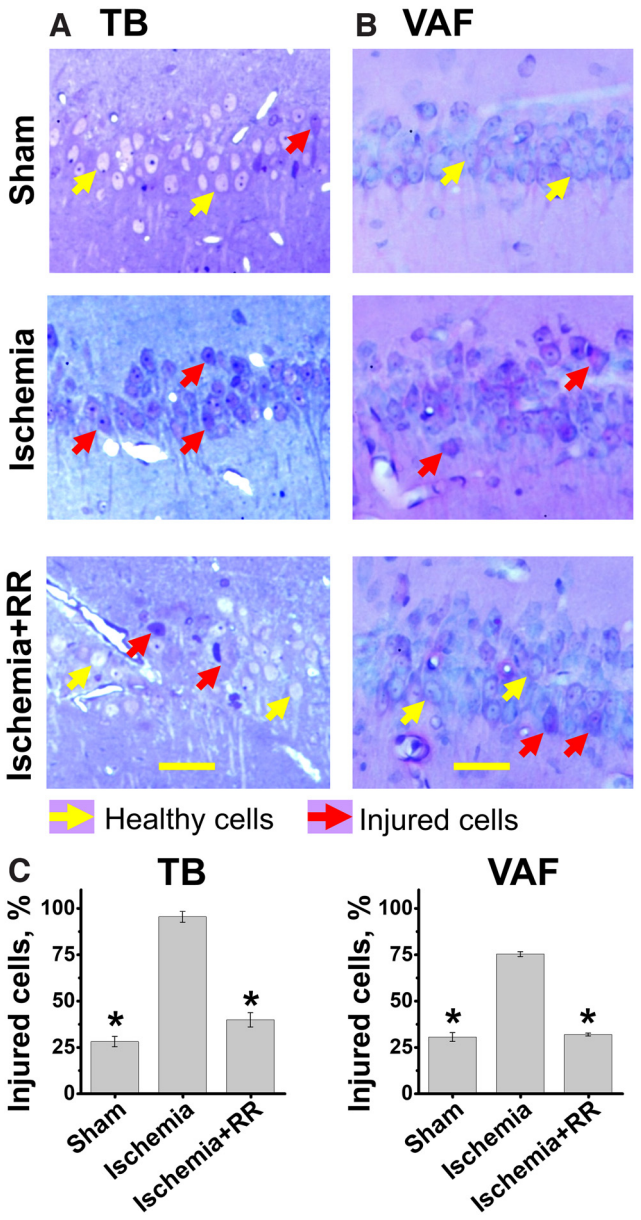

Figure 7. MCU inhibition attenuates neuronal injury in CA1 pyramidal neurons induced by transient global ischemia. Rats were subjected to sham treatment, transient global ischemia induced by CA (8 min), or CA followed by intravenous treatment with RR (2.5 mg/kg). After 4 h of recovery, rats were killed, and brain tissue collected for histologic examination. To assess injury, slices were stained with TB or subjected to a modified acid fuchsin labeling procedure (VAF). ***A***, Representative images of TB-stained slices. CA1 regions of hippocampal slices were photographed under the light microscope. Scale bar, 50 µm. While most neurons appear intact (shown with yellow arrow) in sham slices, note the substantial numbers of TB-stained neurons after ischemia (red arrows). Further, injury was largely attenuated in neurons from animals treated with RR. ***B***, Representative images of VAF-stained slices. The majority of neurons appear healthy (yellow arrows) in slices from sham-treated animals, but after ischemia most neurons are injured (red arrows) and have VAF labeling in cytoplasm. Injury was significantly reversed in animals treated with RR. ***C***, Quantitative assessment. Left, TB stain. Right, VAF labeling. All neurons were blindly analyzed and rated as intact or injured, and the percentages of CA1 neurons determined to be injured within each animal were calculated. The number of injured cells was far greater in the CA1 zone of animals subjected to ischemia than after sham treatment, and RR administration greatly diminished neuronal injury. Error bars indicate mean (±SE) from 3 independent animals (with ≥3 sections analyzed for each animal). Number of TB-stained injured neurons: sham treatment 27.9 ± 2.8%; ischemia 95.4 ± 2.9%; ischemia+RR 39.7 ± 3.9%. Number of VAF-stained injured neurons: sham treatment 25.3 ± 4.2%; ischemia 69.7 ± 5.7%; ischemia+RR 28.7 ± 6.2%. *$p < 0.01$ versus ischemia (one-way ANOVA).

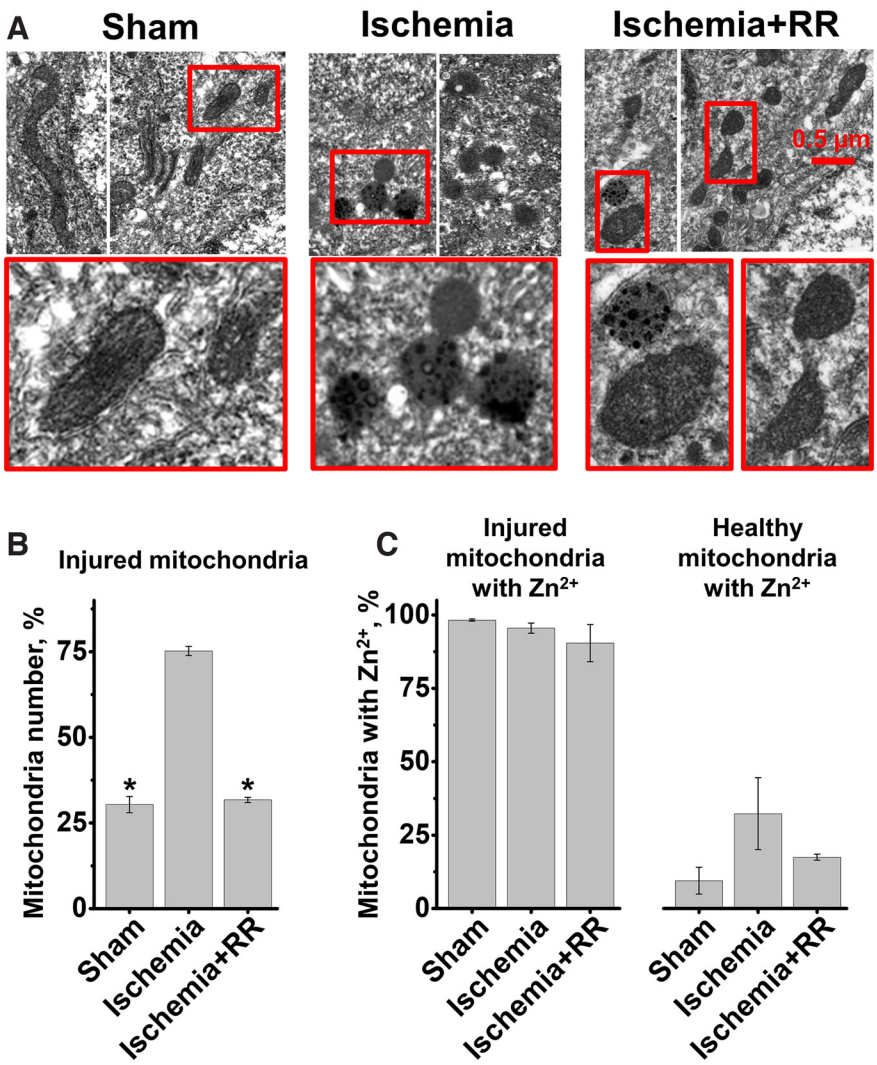

Figure 8. MCU inhibition decreases mitochondrial structural damage and Zn^{2+} accumulation evoked by ischemia/reperfusion. Rats were subjected to sham treatment, ischemia induced by CA, or ischemia followed by intravenous injection of RR (2.5 mg/kg). Four hours later, rats were killed, brains fixed with 4% PFA, and subjected to Timm's staining. ***A***, Appearance of mitochondria from rats subjected to indicated treatment. Representative EM images show healthy mitochondria with normal morphology, intact intramitochondrial crista structures, and membranes in sham-treated animals, while mitochondria from CA rats are swollen, fragmented, and have rounded morphology and disrupted membranes. Note clearly visible increased numbers of healthy mitochondria with improved morphology and membrane structure in rats treated with RR after CA. Also, most of the damaged mitochondria show Zn^{2+} (visualized by Timm's stain as electron dense spots). ***B***, ***C***, Quantitative measurements. ***B***, Bar graphs represent average numbers (as percent of total mitochondria ± SE) of injured mitochondria (sham 30.4 ± 2.4%; ischemia 75.2 ± 1.3%; ischemia+RR 31.7 ± 0.8%). ***C***, Bar graphs represent percent of mitochondria that exhibited substantial amounts of zinc staining. Left, Number of injured mitochondria containing Zn^{2+}, as percentage of injured mitochondria (sham 98.2 ± 0.4%; ischemia 95.5 ± 1.7%; ischemia+RR 90.4 ± 6.3%). Right, Number of healthy mitochondria with Zn^{2+}, as percentage of healthy mitochondria (sham treatment 9.5 ± 4.6%; ischemia 32.3 ± 12.3%; ischemia+RR 17.5 ± 1%). Each bar comprises measurements from 3 animals per treatment condition. Bars represent mean (±SE) from 3 independent animals (with >100 mitochondria counted per each condition). *$p < 0.01$ versus ischemia (one-way ANOVA).

right) in all three conditions contained Zn^{2+} deposits (visible as electron dense spots). However, even visually healthy-appearing mitochondria from ischemic animals contained Zn^{2+} in a greater proportion (~30% vs ~9% in sham-treated animals; Fig. 8*C*, right). Treatment with RR after ischemia markedly diminished Zn^{2+} accumulation in all mitochondria, both intact and damaged (ischemia 79.8 ± 1.7%; sham 36.4 ± 3%, $p < 0.01$ vs ischemia; ischemia+RR 40.7 ± 4.1%, $p < 0.01$ vs ischemia one-way ANOVA) and decreased mitochondrial injury (Fig. 8).

Discussion

As noted, we have found progressive and long-lasting Zn^{2+} accumulation in mitochondria of CA1 pyramidal neurons to occur after ischemia (Medvedeva et al., 2017; Yin et al., 2019). Present studies are the first to examine effects of this mitochondrial Zn^{2+} accumulation on mitochondrial function and synaptic activity in CA1 neurons in slice over several hours after an ischemic episode. We found that a short episode of OGD causes distinct changes in spontaneous synaptic activity and evokes delayed and persistent loss of $\Delta\Psi_m$ in CA1 hippocampal neurons. These changes seems to be specifically catalyzed by Zn^{2+} entry into mitochondria via the MCU, since they are markedly attenuated by either MCU blockade or Zn^{2+} chelation after the ischemic episode. Furthermore, the short OGD episodes lead to considerable delayed swelling and fragmentation of mitochondria, which is also largely prevented by postischemic MCU inhibition. Finally, in early test of principle studies in an *in vivo* rat CA model of ischemia, we found that administration of an MCU inhibitor after ischemia appears to diminish mitochondrial Zn^{2+} accumulation, mitochondrial disruption, and delayed neuronal injury (Fig. 9).

Role of Zn^{2+}-mitochondria interactions in ischemic injury

Multiple lines of evidence support a critical contribution of Zn^{2+} to ischemic injury. Specifically, large amounts of free Zn^{2+} were found to accumulate after ischemia in some vulnerable groups of neurons, including hippocampal CA1 neurons (Tonder et al., 1990; Koh et al., 1996). Furthermore, Zn^{2+} chelators were protective in both *in vitro* and *in vivo* ischemic models (Koh et al., 1996; Yin et al., 2002; Calderone et al., 2004; Medvedeva et al., 2009; Medvedeva and Weiss, 2014).

While there is considerable Zn^{2+} in the brain, the majority of it is normally bound or sequestered, such that free Zn^{2+} is very low (subnanomolar). One important Zn^{2+} pool comprises Zn^{2+} sequestered in synaptic vesicles, from which it is released on strong synaptic stimulation, and can enter neurons through certain Ca^{2+} permeable channels (Weiss et al., 2000; Shuttleworth and Weiss, 2011). Another important Zn^{2+} pool is that bound to cytosolic buffering proteins (in neurons largely comprising metallothionein-III [MT-III]) from which it is released on metabolic perturbations (oxidative stress and acidosis) as occur during ischemia/reperfusion (Maret and Vallee, 1998; L. J. Jiang et al., 2000; Maret, 2011). Zn^{2+} mobilization from this pool appears to contribute considerably to ischemic injury in CA1 neurons (Lee et al., 2003;

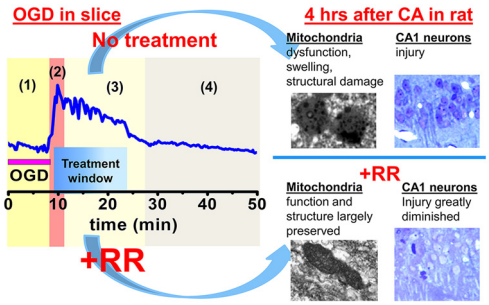

Figure 9. Mitochondrial Zn^{2+} uptake through the MCU after ischemia is a target for neuroprotection. Sequence of events occurring during ischemia/reperfusion: (1) During early OGD, Zn^{2+} enters into the cell and is released from MT-III. Zn^{2+} accumulates in mitochondria, which start to depolarize. (2) Mitochondria abruptly depolarize releasing Zn^{2+} into cytosol; (3) with reperfusion, mitochondria repolarize and reuptake the Zn^{2+}. This stage is targeted to prevent the Zn^{2+} uptake and resulting injury. (4) Zn^{2+} stays in CA1 (but not CA3) mitochondria for a prolonged period of time. Blue trace represents changes in cytoplasmic [Zn^{2+}] measured with Zn^{2+} sensitive indicator FluoZin-3. Representative images on the right show EM microphotograph of CA1 mitochondria and bright field images of TB labeled CA1 neurons 4 h after global ischemia (top) and 4 h after ischemia+RR (bottom) in rat.

Medvedeva et al., 2017; Ji et al., 2019). Our recent findings using short ischemia in hippocampal slice suggest that Zn^{2+}, which is progressively released from MT-III during ischemia/reperfusion, permeates the MCU, accumulating in CA1 mitochondria (Medvedeva et al., 2017).

It is apparent that mitochondria are key players in ischemic neuronal injury and were proposed as important targets for treatment (Liu and Murphy, 2009; Sims and Muyderman, 2010). Changes in brain mitochondrial structure after transient global ischemia have been detected early (during first few hours) (Solenski et al., 2002; Bonanni et al., 2006; Yin et al., 2019) with more severe damage hours and days later (Colbourne et al., 1999).

While the precise mechanisms through which Zn^{2+} promotes neurodegeneration are not defined, multiple studies have highlighted mitochondria as a target for Zn^{2+}. Zn^{2+} is taken up into mitochondria via the MCU (Saris and Niva, 1994; Malaiyandi et al., 2005; Clausen et al., 2013; Medvedeva and Weiss, 2014; Ji et al., 2020), and affects their function with much greater potency than Ca^{2+}, causing mitochondrial depolarization, ROS generation, and potent induction of swelling, probably because of activation of the mPTP (Sensi et al., 1999, 2000; D. Jiang et al., 2001; Ji and Weiss, 2018). Indeed, studies on isolated mitochondria have demonstrated potent mPTP activation after Zn^{2+} entry through the MCU (D. Jiang et al., 2001; Gazaryan et al., 2007; Ji et al., 2019). Although mechanisms of these effects are incompletely understood, Zn^{2+} was found to induce irreversible inhibition of several mitochondrial enzymes of energy production and antioxidant defense, likely contributing to both mitochondrial ROS production and mPTP induction (Gazaryan et al., 2002, 2007). The mPTP induction, in turn, triggers release of apoptotic mediators, including cytochrome C and apoptosis-inducing factor (D. Jiang et al., 2001) that contribute to activation of downstream apoptotic injury pathways (Bernardi, 1999; Crompton, 1999; Fatokun et al., 2014).

Notably, mitochondria seem to be critically involved in the delayed selective degeneration of CA1 pyramidal neurons after transient ischemia. These neurons show mitochondrial swelling with release of cytochrome C into the cytoplasm beginning within hours of ischemia, followed by caspase-3 activation, and with neurodegeneration and associated prominent DNA fragmentation, occurring over the next days (Antonawich, 1999; Nakatsuka et al., 1999; Ouyang et al., 1999; Sugawara et al., 1999). In addition, treatment with the Zn^{2+} chelator, Ca-EDTA, decreased cytochrome C release in CA1 neurons after ischemia (Calderone et al., 2004) supporting a Zn^{2+} contribution to the activation of this apoptotic pathway. Our recent study using the slice OGD model of ischemia found that mitochondrial Zn^{2+} uptake appears to contribute to ROS production during ischemia (Medvedeva and Weiss, 2014). Present findings that Zn^{2+} accumulation into CA1 mitochondria after short ischemia contributes to delayed loss of $\Delta\Psi_m$, mitochondrial swelling, and neuronal injury support the hypothesis that prolonged Zn^{2+} accumulation in CA1 neuronal mitochondria after ischemia represents a critical and targetable event contributing to their delayed degeneration.

Alterations in synaptic function after OGD

Alterations in synaptic structure and function have been observed hours and days after an ischemic event. These include remodeling of synaptic networks and increases in amplitude of evoked postsynaptic potentials in the CA1 area, with postsynaptic LTP detected in CA3-CA1 synapses in hippocampal slices (Jourdain et al., 2002; Crepel et al., 2003; Ai and Baker, 2006; Neumann et al., 2013). Structural changes at both presynaptic and postsynaptic levels that evolve after ischemia include postsynaptic spine swelling, decreased synaptic spine density, depletion of presynaptic vesicle pools, and decreased numbers of mitochondria in CA1 presynaptic terminals (Kovalenko et al., 2006; Radenovic et al., 2011; Neumann et al., 2013).

These observations are compatible with our findings of alterations in synaptic activity, with increases in frequency of excitatory SPSCs recorded in CA1 neurons 2-3 h after OGD followed by progressive quieting of synaptic function. We found that these alterations depend on Zn^{2+} accumulation into mitochondria, since they were largely prevented by MCU inhibition or Zn^{2+} chelation. It is thus likely that mitochondrial damage and dysfunction catalyzed by Zn^{2+} accumulation contributes to observed changes in synaptic activity.

Zn^{2+} uptake through the MCU: a target for neuroprotective treatment

Despite being a leading cause of death and disability, treatment of brain ischemia is largely limited to restoration of blood flow. Multiple past studies have proposed that massive neuronal Ca^{2+} loading via NMDA channels constitutes a promising target for neuroprotection. But glutamate-triggered Ca^{2+} overload occurs primarily during acute ischemia. However, since ischemia cannot be predicted, the main opportunity for intervention is after ischemia has been terminated and blood flow restored. If ischemia ends before acute cell death has occurred, neurons initially recover but often die hours or days later. Targeting NMDA receptors after an episode of ischemia did not help in preventing this delayed cell death (Ikonomidou and Turski, 2002; Hoyte et al., 2004). Thus, other mechanisms, occurring after an acute ischemic episode, need to be targeted. Zn^{2+} accumulation in mitochondria seems to be such a mechanism.

While routes for Zn^{2+} translocation into mitochondria are not completely defined, the MCU appears to be a major route for substantial rapid mitochondrial Zn^{2+} uptake (Malaiyandi et al., 2005; Medvedeva and Weiss, 2014; Ji et al., 2020). Indeed, our recent study found that blocking the MCU prevents the long-lasting mitochondrial Zn^{2+} uptake in CA1 neurons occurring after ischemia (Medvedeva et al., 2017). Present studies

demonstrate that inhibiting the MCU after ischemia has occurred greatly diminishes deleterious changes evoked by ischemia/reperfusion in hippocampal slices, and decreases neuronal and mitochondrial injury after CA in animals. Furthermore, Zn^{2+} chelation (also administered after OGD in slice) had similar effects, supporting the contention that protection is because of preventing Zn^{2+} accumulation in mitochondria. Thus, the occurrence of long-lasting postischemic mitochondrial Zn^{2+} accumulation in vulnerable CA1 hippocampal pyramidal neurons, but not in more resistant CA3 neurons, together with observation of beneficial effects of MCU inhibition or Zn^{2+} chelation after ischemia provides support to the idea that mitochondrial Zn^{2+} accumulation is a critical event occurring after ischemia which leads to delayed neuronal injury. Furthermore, this mechanism can be targeted for neuroprotection and thus may constitute a promising target for development of therapeutic interventions to be delivered after the ischemia has already occurred.

References

Ai J, Baker A (2006) Long-term potentiation of evoked presynaptic response at CA3-CA1 synapses by transient oxygen-glucose deprivation in rat brain slices. Exp Brain Res 169:126–129.

Antonawich FJ (1999) Translocation of cytochrome c following transient global ischemia in the gerbil. Neurosci Lett 274:123–126.

Azadian M, Tian G, Bazrafkan A, Maki N, Rafi M, Chetty N, Desai M, Otarola I, Aguirre F, Zaher SM, Khan A, Suri Y, Wang M, Lopour BA, Steward O, Akbari Y (2020) Overnight caloric restriction prior to cardiac arrest and resuscitation leads to improved survival and neurological outcome in a rodent model. Front Neurosci 14:609670.

Ben-Ari Y, Tremblay E, Ottersen OP (1980a) Injections of kainic acid into the amygdaloid complex of the rat: an electrographic, clinical and histological study in relation to the pathology of epilepsy. Neuroscience 5:515–528.

Ben-Ari Y, Tremblay E, Ottersen OP, Meldrum BS (1980b) The role of epileptic activity in hippocampal and 'remote' cerebral lesions induced by kainic acid. Brain Res 191:79–97.

Bernardi P (1999) Mitochondrial transport of cations: channels, exchangers, and permeability transition. Physiol Rev 79:1127–1155.

Bonanni L, Chachar M, Jover-Mengual T, Li H, Jones A, Yokota H, Ofengeim D, Flannery RJ, Miyawaki T, Cho CH, Polster BM, Pypaert M, Hardwick JM, Sensi SL, Zukin RS, Jonas EA (2006) Zinc-dependent multi-conductance channel activity in mitochondria isolated from ischemic brain. J Neurosci 26:6851–6862.

Calderone A, Jover T, Mashiko T, Noh KM, Tanaka H, Bennett MV, Zukin RS (2004) Late calcium EDTA rescues hippocampal CA1 neurons from global ischemia-induced death. J Neurosci 24:9903–9913.

Clausen A, McClanahan T, Ji SG, Weiss JH (2013) Mechanisms of rapid reactive oxygen species generation in response to cytosolic Ca^{2+} or Zn^{2+} loads in cortical neurons. PLoS One 8:e83347.

Colbourne F, Sutherland GR, Auer RN (1999) Electron microscopic evidence against apoptosis as the mechanism of neuronal death in global ischemia. J Neurosci 19:4200–4210.

Cole TB, Wenzel HJ, Kafer KE, Schwartzkroin PA, Palmiter RD (1999) Elimination of zinc from synaptic vesicles in the intact mouse brain by disruption of the ZnT3 gene. Proc Natl Acad Sci USA 96:1716–1721.

Crepel V, Epsztein J, Ben-Ari Y (2003) Ischemia induces short- and long-term remodeling of synaptic activity in the hippocampus. J Cell Mol Med 7:401–407.

Crompton M (1999) The mitochondrial permeability transition pore and its role in cell death. Biochem J 341:233–249.

Crouzet C, Wilson RH, Bazrafkan A, Farahabadi MH, Lee D, Alcocer J, Tromberg BJ, Choi B, Akbari Y (2016) Cerebral blood flow is decoupled from blood pressure and linked to EEG bursting after resuscitation from cardiac arrest. Biomed Opt Express 7:4660–4673.

Crouzet C, Wilson RH, Lee D, Bazrafkan A, Tromberg BJ, Akbari Y, Choi B (2020) Dissociation of cerebral blood flow and femoral artery blood pressure pulsatility after cardiac arrest and resuscitation in a rodent model: implications for neurological recovery. J Am Heart Assoc 9:e012691.

Danscher G, Zimmer J (1978) An improved Timm sulphide silver method for light and electron microscopic localization of heavy metals in biological tissues. Histochemistry 55:27–40.

De Biasi S, Bendotti C (1998) A simplified procedure for the physical development of the sulphide silver method to reveal synaptic zinc in combination with immunocytochemistry at light and electron microscopy. J Neurosci Methods 79:87–96.

Duchen MR, Surin A, Jacobson J (2003) Imaging mitochondrial function in intact cells. Methods Enzymol 361:353–389.

Fatokun AA, Dawson VL, Dawson TM (2014) Parthanatos: mitochondrial-linked mechanisms and therapeutic opportunities. Br J Pharmacol 171:2000–2016.

Gazaryan IG, Krasnikov BF, Ashby GA, Thorneley RN, Kristal BS, Brown AM (2002) Zinc is a potent inhibitor of thiol oxidoreductase activity and stimulates reactive oxygen species production by lipoamide dehydrogenase. J Biol Chem 277:10064–10072.

Gazaryan IG, Krasinskaya IP, Kristal BS, Brown AM (2007) Zinc irreversibly damages major enzymes of energy production and antioxidant defense prior to mitochondrial permeability transition. J Biol Chem 282:24373–24380.

Hosseini M, Wilson RH, Crouzet C, Amirhekmat A, Wei KS, Akbari Y (2020) Resuscitating the globally ischemic brain: TTM and beyond. Neurotherapeutics 17:539–562.

Hoyte L, Barber PA, Buchan AM, Hill MD (2004) The rise and fall of NMDA antagonists for ischemic stroke. Curr Mol Med 4:131–136.

Ikonomidou C, Turski L (2002) Why did NMDA receptor antagonists fail clinical trials for stroke and traumatic brain injury? Lancet Neurol 1:383–386.

Ji SG, Weiss JH (2018) Zn(2+)-induced disruption of neuronal mitochondrial function: synergism with Ca(2+), critical dependence upon cytosolic Zn(2+) buffering, and contributions to neuronal injury. Exp Neurol 302:181–195.

Ji SG, Medvedeva YV, Wang HL, Yin HZ, Weiss JH (2019) Mitochondrial Zn(2+) accumulation: a potential trigger of hippocampal ischemic injury. Neuroscientist 25:126–138.

Ji SG, Medvedeva YV, Weiss JH (2020) Zn(2+) entry through the mitochondrial calcium uniporter is a critical contributor to mitochondrial dysfunction and neurodegeneration. Exp Neurol 325:113161.

Jiang D, Sullivan PG, Sensi SL, Steward O, Weiss JH (2001) Zn(2+) induces permeability transition pore opening and release of pro-apoptotic peptides from neuronal mitochondria. J Biol Chem 276:47524–47529.

Jiang LJ, Vasak M, Vallee BL, Maret W (2000) Zinc transfer potentials of the alpha- and beta-clusters of metallothionein are affected by domain interactions in the whole molecule. Proc Natl Acad Sci USA 97:2503–2508.

Jourdain P, Nikonenko I, Alberi S, Muller D (2002) Remodeling of hippocampal synaptic networks by a brief anoxia-hypoglycemia. J Neurosci 22:3108–3116.

Kang YJ, Tian G, Bazrafkan A, Farahabadi MH, Azadian M, Abbasi H, Shamaoun BE, Steward O, Akbari Y (2017) Recovery from coma post-cardiac arrest is dependent on the orexin pathway. J Neurotrauma 34:2823–2832.

Kirino T (1982) Delayed neuronal death in the gerbil hippocampus following ischemia. Brain Res 239:57–69.

Koh JY, Suh SW, Gwag BJ, He YY, Hsu CY, Choi DW (1996) The role of zinc in selective neuronal death after transient global cerebral ischemia. Science 272:1013–1016.

Kovalenko T, Osadchenko I, Nikonenko A, Lushnikova I, Voronin K, Nikonenko I, Muller D, Skibo G (2006) Ischemia-induced modifications in hippocampal CA1 stratum radiatum excitatory synapses. Hippocampus 16:814–825.

Lee JY, Kim JH, Palmiter RD, Koh JY (2003) Zinc released from metallothionein-iii may contribute to hippocampal CA1 and thalamic neuronal death following acute brain injury. Exp Neurol 184:337–347.

Liu RR, Murphy TH (2009) Reversible cyclosporin A-sensitive mitochondrial depolarization occurs within minutes of stroke onset in mouse somatosensory cortex in vivo: a two-photon imaging study. J Biol Chem 284:36109–36117.

Malaiyandi LM, Vergun O, Dineley KE, Reynolds IJ (2005) Direct visualization of mitochondrial zinc accumulation reveals uniporter-dependent and -independent transport mechanisms. J Neurochem 93:1242–1250.

Maret W (2011) Redox biochemistry of mammalian metallothioneins. J Biol Inorg Chem 16:1079–1086.

Maret W, Vallee BL (1998) Thiolate ligands in metallothionein confer redox activity on zinc clusters. Proc Natl Acad Sci USA 95:3478–3482.

Medvedeva YV, Weiss JH (2014) Intramitochondrial Zn(2+) accumulation via the Ca(2+) uniporter contributes to acute ischemic neurodegeneration. Neurobiol Dis 68:137–144.

Medvedeva YV, Lin B, Shuttleworth CW, Weiss JH (2009) Intracellular Zn^{2+} accumulation contributes to synaptic failure, mitochondrial depolarization, and cell death in an acute slice oxygen-glucose deprivation model of ischemia. J Neurosci 29:1105–1114.

Medvedeva YV, Ji SG, Yin HZ, Weiss JH (2017) Differential vulnerability of CA1 versus CA3 pyramidal neurons after ischemia: possible relationship to sources of Zn^{2+} accumulation and its entry into and prolonged effects on mitochondria. J Neurosci 37:726–737.

Nakatsuka H, Ohta S, Tanaka J, Toku K, Kumon Y, Maeda N, Sakanaka M, Sakaki S (1999) Release of cytochrome c from mitochondria to cytosol in gerbil hippocampal CA1 neurons after transient forebrain ischemia. Brain Res 849:216–219.

Neumann JT, Cohan CH, Dave KR, Wright CB, Perez-Pinzon MA (2013) Global cerebral ischemia: synaptic and cognitive dysfunction. Curr Drug Targets 14:20–35.

Ordy JM, Wengenack TM, Bialobok P, Coleman PD, Rodier P, Baggs RB, Dunlap WP, Kates B (1993) Selective vulnerability and early progression of hippocampal CA1 pyramidal cell degeneration and GFAP-positive astrocyte reactivity in the rat four-vessel occlusion model of transient global ischemia. Exp Neurol 119:128–139.

Ouyang YB, Tan Y, Comb M, Liu CL, Martone ME, Siesjo BK, Hu BR (1999) Survival- and death-promoting events after transient cerebral ischemia: phosphorylation of Akt, release of cytochrome C and activation of caspase-like proteases. J Cereb Blood Flow Metab 19:1126–1135.

Park J, Trinh VN, Sears-Kraxberger I, Li KW, Steward O, Luo ZD (2016) Synaptic ultrastructure changes in trigeminocervical complex posttrigeminal nerve injury. J Comp Neurol 524:309–322.

Petito CK, Feldmann E, Pulsinelli WA, Plum F (1987) Delayed hippocampal damage in humans following cardiorespiratory arrest. Neurology 37:1281–1286.

Radenovic L, Korenic A, Maleeva G, Osadchenko I, Kovalenko T, Skibo G (2011) Comparative ultrastructural analysis of mitochondria in the CA1 and CA3 hippocampal pyramidal cells following global ischemia in Mongolian gerbils. Anat Rec (Hoboken) 294:1057–1065.

Saris NE, Niva K (1994) Is Zn^{2+} transported by the mitochondrial calcium uniporter? FEBS Lett 356:195–198.

Sensi SL, Yin HZ, Weiss JH (2000) AMPA/kainate receptor-triggered Zn^{2+} entry into cortical neurons induces mitochondrial Zn^{2+} uptake and persistent mitochondrial dysfunction. Eur J Neurosci 12:3813–3818.

Sensi SL, Yin HZ, Carriedo SG, Rao SS, Weiss JH (1999) Preferential Zn^{2+} influx through Ca^{2+}-permeable AMPA/kainate channels triggers prolonged mitochondrial superoxide production. Proc Natl Acad Sci USA 96:2414–2419.

Sensi SL, Ton-That D, Sullivan PG, Jonas EA, Gee KR, Kaczmarek LK, Weiss JH (2003) Modulation of mitochondrial function by endogenous Zn^{2+} pools. Proc Natl Acad Sci USA 100:6157–6162.

Shuttleworth CW, Weiss JH (2011) Zinc: new clues to diverse roles in brain ischemia. Trends Pharmacol Sci 32:480–486.

Sims NR, Muyderman H (2010) Mitochondria, oxidative metabolism and cell death in stroke. Biochim Biophys Acta 1802:80–91.

Solenski NJ, diPierro CG, Trimmer PA, Kwan AL, Helm GA, Helms GA (2002) Ultrastructural changes of neuronal mitochondria after transient and permanent cerebral ischemia. Stroke 33:816–824.

Sugawara T, Fujimura M, Morita-Fujimura Y, Kawase M, Chan PH (1999) Mitochondrial release of cytochrome c corresponds to the selective vulnerability of hippocampal CA1 neurons in rats after transient global cerebral ischemia. J Neurosci 19:RC39.

Tanaka S, Kondo S, Tanaka T, Yonemasu Y (1988) Long-term observation of rats after unilateral intra-amygdaloid injection of kainic acid. Brain Res 463:163–167.

Tonder N, Johansen FF, Frederickson CJ, Zimmer J, Diemer NH (1990) Possible role of zinc in the selective degeneration of dentate hilar neurons after cerebral ischemia in the adult rat. Neurosci Lett 109:247–252.

Victorov IV, Prass K, Dirnagl U (2000) Improved selective, simple, and contrast staining of acidophilic neurons with vanadium acid fuchsin. Brain Res Brain Res Protoc 5:135–139.

Weiss JH, Sensi SL, Koh JY (2000) Zn(2+): a novel ionic mediator of neural injury in brain disease. Trends Pharmacol Sci 21:395–401.

Wudarczyk J, Debska G, Lenartowicz E (1999) Zinc as an inducer of the membrane permeability transition in rat liver mitochondria. Arch Biochem Biophys 363:1–8.

Yin HZ, Sensi SL, Ogoshi F, Weiss JH (2002) Blockade of Ca^{2+}-permeable AMPA/kainate channels decreases oxygen-glucose deprivation-induced Zn^{2+} accumulation and neuronal loss in hippocampal pyramidal neurons. J Neurosci 22:1273–1279.

Yin HZ, Wang HL, Ji SG, Medvedeva YV, Tian G, Bazrafkan AK, Maki NZ, Akbari Y, Weiss JH (2019) Rapid intramitochondrial Zn^{2+} accumulation in CA1 hippocampal pyramidal neurons after transient global ischemia: a possible contributor to mitochondrial disruption and cell death. J Neuropathol Exp Neurol 78:655–664.

Zola-Morgan S, Squire LR, Amaral DG (1986) Human amnesia and the medial temporal region: enduring memory impairment following a bilateral lesion limited to field CA1 of the hippocampus. J Neurosci 6:2950–2967.